Photochemical Properties of UV Filter Molecules of the Human Eye

Tsentalovich, Y. P.; Sherin, Petr; Kopylova, L. V.; Cherepanov, I. V.; Grilj, Jakob; Vauthey, Eric

Photochemical Properties of UV Filter Molecules of the Human Eye

Yuri P. Tsentalovich,[*,1] Peter S. Sherin,[1,2] Lyudmila V. Kopylova,[1] Ivan V. Cherepanov,[1,3] Jakob Grilj,[2] and Eric Vauthey*[*,2]*

Purpose. To compare the photochemical properties of UV filter molecules present in the human lens (kynurenine, KN; 3-hydroxykynurenine, 3OHKN; 3-hydroxykynurenine *O*-β-D-glucoside, 3OHKG; 4-(2-aminophenyl)-4-oxobutanoic acid, AHA; and glutathionyl-kynurenine, GSH-KN) with the use of the following parameters: excited singlet lifetime τ_S, fluorescence quantum yield Φ_{fl}, triplet quantum yield Φ_T, and photodecomposition quantum yield Φ_{dec}.

Methods. The excited singlet lifetimes were measured with the use of fluorescence upconversion (time resolution, 210 fs) and pump-probe transient absorption (time resolution, 200 fs) methods. The fluorescence quantum yields were determined relative to an aqueous solution of quinine bisulfate. The triplet quantum yields were measured with the use of nanosecond laser flash photolysis. The photodecomposition quantum yields were determined by steady state photolysis followed by the high-performance liquid chromatography analysis.

Results. The secondary UV filters—AHA and GSH-KN are better photosensitizers than the primary ones—KN, 3OHKN and 3OHKG: the singlet state lifetimes of the secondary UV filters are longer, and the quantum yields of fluorescence and triplet state formation are higher.

Conclusions. With aging, the ratio primary/secondary UV filters in the human lens decreases from approximately 10:1 to 2:1. The obtained results demonstrate that the quality of the secondary UV filters is inferior compared to the primary ones, which may result in a higher susceptibility of old lenses to UV light. That might be an important factor for the development of the age-related cataract. (*Invest Ophthalmol Vis Sci.* 2011;52:7687–7696) DOI:10.1167/iovs.11-8120

The human eye lens contains low-molecular-weight compounds that absorb UV light in the 300 to 400 nm region of the spectrum, protecting the lens and retina from UV-induced photodamage. The most abundant UV filter molecules are kynurenine (KN), 3-hydroxykynurenine (3OHKN), 3-hydroxykynurenine *O*-β-D-glucoside (3OHKG), 4-(2-amino-3-hydroxyphenyl)-4-oxobutanoic acid glycoside (AHBG), and glutathionyl-3-hydroxykynurenine glycoside (GSH-3OHKG).[1–8] By origin, UV filters can be divided into primary and secondary filters. The primary filters—KN, 3OHKN, and 3OHKG—are enzymatically synthesized from tryptophan in the epithelial cells of the lens and are transported to the lens core by diffusion.[1,9] These compounds can undergo spontaneous deamination, forming unsaturated carboxyketoalkenes.[10,11] The reduction of deaminated 3OHKG leads to the formation of AHBG, and the addition of the reduced glutathione to deaminated 3OHKG yields GSH-3OHKG.[10,12,13] The concentrations of these UV filters in the lens vary with age. In young lenses, the levels of the primary filters 3OHKG, KN, and 3OHKN are high, whereas GSH-3OHKG is practically absent.[5] With age, the concentrations of 3OHKG, KN, and 3OHKN decay by approximately 12% per decade, whereas the concentration of GSH-3OHKG increases, and, in old lenses, it becomes as high as the concentration of the most abundant UV filter, 3OHKG.[5] Thus, the concentration ratio of primary/secondary filters decreases with age. If the photochemical properties of primary and secondary UV filters differ, that may influence the susceptibility of the eye to UV irradiation.

The goal of this work was to compare the photochemical properties and photostability of primary and secondary UV filters. Among the major UV filters found in the human lens, only the photochemistry of KN has been studied in detail,[11,14–21] some data can be found on 3OHKN[14,17,19,21–23] and glutathionyl-kynurenine[19,24] (GSH-KN), whereas the photochemical properties of 3OHKG and AHBG have not been reported yet. It has been shown that the S_1 lifetime of KN amounts to 30 ps in aqueous solutions, increases by more than one order of magnitude in alcohols, and exceeds 1 ns in aprotic solvents such as DMSO and DMF.[21] The main channel of the S_1 state deactivation in protic solvents is solvent-assisted internal conversion, based on the hydrogen bonding interactions between KN in the S_1 state and the solvent molecules. Excitation of KN results in an increase in the electron density on the carbonyl oxygen that augments the acidity of the amino group and the basicity of the carbonyl group, which, in turn, leads to an enhancement of their hydrogen bonding ability. The stretching vibrations of the hydrogen bonds act as accepting modes for the $S_1 \rightarrow S_0$ nonradiative transition and thus the electronic energy dissipates through the hydrogen bonds as vibrational energy.[21] In an extreme case of hydrogen bond stretching, an intermolecular proton transfer may occur, result-

From the [1]International Tomography Center, SB (Siberian Branch), Russian Academy of Science (RAS), Novosibirsk, Russia; the [2]Department of Physical Chemistry, University of Geneva, Geneva, Switzerland; and the [3]Department of Physics, Novosibirsk State University, Novosibirsk, Russia.

Supported by Ministry of Education of Russian Federation, state contract 14.740.11.0758; Russian Foundation for Basic Research Projects (11-04-00143-a, 11-03-00296-a, and 11-04-12006-ofi-m-2011); the President of the Russian Federation Grant NSh-7643.2010.3; the Division of Chemistry and Material Science, Russian Academy of Sciences; a Government of Moscow Program ("New Methods and Technologies of Early Diagnostics and treatment of Oncological and Other Dangerous Diseases"); Fonds National Suisse de la Recherche Scientifique Project 200020-115942; and the University of Geneva.

Submitted for publication June 24, 2011; revised August 1, 2011; accepted August 1, 2011.

Disclosure: **Y.P. Tsentalovich**, None; **P.S. Sherin**, None; **L.V. Kopylova**, None; **I.V. Cherepanov**, None; **J. Grilj**, None; **E. Vauthey**, None

*Each of the following is a corresponding author: Yuri P. Tsentalovich, International Tomography Center, 630090, Institutskaya 3a, Novosibirsk, Russia; yura@tomo.nsc.ru.

Eric Vauthey, University of Geneva, 30 quai Ernest-Ansermet, CH-1211 Geneva 4, Switzerland; eric.vauthey@unige.ch.

ing in the protonation of the carbonyl group and deprotonation of the amino group and followed by ultrafast back proton transfer. Because all UV filter compounds have similar structures, one can expect the same mechanisms of S_1 state deactivation, but the rate constants and quantum yields of various deactivation channels of the S_1 state can differ for the different UV filters.

Whereas KN and 3OHKN are commercially available, the other UV filters—3OHKG, 4-(2-aminophenyl)-4-oxobutanoic acid (AHA, an analog of AHBG) and glutathionyl-kynurenine (GSH-KN, an analog of GSH-3OHKG)— had to be synthesized. The following parameters have been taken as a measure of the quality of the UV filters: excited singlet lifetime τ_S, fluorescence quantum yield Φ_{fl}, triplet quantum yield Φ_T, and photodecomposition quantum yield Φ_{dec}. The measurements for all five UV filters were performed under as similar conditions as possible to minimize systematic errors. The obtained results are discussed in relation to the abundance of primary and secondary UV filters in lenses of different age.

METHODS

Materials

D,L-Kynurenine (KN) was purchased from Fluka (Buchs, Switzerland), and 3-hydroxy-D,L-kynurenine (3OHKN) was obtained from Sigma-Aldrich (St. Louis, MO) and purified by semipreparative HPLC. Acetobromo-α-D-glucose (ABG; Sigma-Aldrich) was used as received. H_2O was distilled and deionized. Methanol was distilled and dried over molecular sieves.

The KN adduct of glutathione (GSH-KN, Chart 1) was synthesized according to a method[19,25,26] described earlier: D,L-Kynurenine sulfate salt (33.3) mg was dissolved in 20 mL of phosphate buffer at pH 9.5, GSH was added in a 10-fold molar excess. The pH was readjusted to 9.5 with NaOH. The solution, placed in a glass vial, was bubbled with argon, sealed, and incubated at 37°C for 48 hours. After adjusting the pH to 4.5 with hydrochloric acid (HCl), the reaction mixture was separated by semipreparative HPLC. The adduct-containing fraction was lyophilized and stored at −18°C.

The synthesis of 3OHKG was performed similarly to the procedure described elsewhere.[27,28] 3OHKN (14.6 mg) was dissolved in 2 mL MeOH, the pH was adjusted to 10.6 by the addition of NaOH dissolved in MeOH. ABG (95 mg) was added, the pH was readjusted to 10.6 and maintained between 10.4 and 10.9 during the whole synthesis. The reaction mixture was stirred with a magnetic stirrer for 7 hours. As the pH value stabilized, more portions of ABG were added to the solution, the total amount of added ABG being approximately 400 mg. The reaction was neutralized with HCl and the resulting mixture was rotovapped to dryness. The water-soluble fraction was extracted with approximately 5 mL H_2O, and separated by semipreparative HPLC. The 3OHKG-containing fraction was collected, lyophilized, and stored at −18°C.

The synthesis of AHA was performed similarly to a published procedure.[7] CKA (57.4 mg) was dissolved in a mixture composed of 8 mL ethyl acetate and 14 μL acetic acid. PtO_2 (3.5 mg) was added. The solution was bubbled with hydrogen and stirred with a magnetic stirrer for 9 hours. The reaction mixture was filtered and rotovapped to dryness. The water-soluble fraction was extracted with approximately 5 mL H_2O, and separated by semipreparative HPLC. The AHA-containing fraction was collected, lyophilized, and stored at −18°C.

The identities of GSH-KN, 3OHKG, and AHA were verified by mass spectrometry with the use of an ion trap (Esquire6000; Bruker Daltonics, Billerica, MA). The acquisition parameters were the following: positive scan mode in the range of 50 to 1000 *m/z*, V_{cap} 4000 V; nebulizer pressure, 15 psi; and drying gas (N_2) temperature, 300°C. The following ions were detected: for GSH-KN: *m/z* 499 (molecular ion), fragments *m/z* 481 (—H_2O), *m/z* 424 (—$C_2H_5NO_2$), *m/z* 370 (—$C_5H_7NO_3$), *m/z* 352 (—$C_5H_{11}N_2O_3$), *m/z* 259 (—$C_{11}H_{14}NO_3S$); for 3OHKG: molecular ion *m/z* 387, fragments *m/z* 370 (—NH_3), *m/z* 225 (—glucose); for AHA: molecular ion *m/z* 194, fragments *m/z* 176 (—H_2O), *m/z* 148 (—CH_2O_2), and *m/z* 94 (—$C_4H_4O_3$).

High-Performance Liquid Chromatography

HPLC separations were performed with a chromatograph (LC 1200; Agilent, Santa Clara, CA) equipped with an automatic gradient pump and a UV-Vis diode array detector.

The HPLC analysis of the irradiated samples was performed on a 4.6 × 150-mm, 5-μm C18 analytical column (ZORBAX Eclipse XBD; Aglient), using an acetonitrile/0.05% (vol/vol) TFA in H_2O gradient. The acetonitrile percentage in the gradient was 0% (0–5 minutes), 0% to 20% (5–5.01 minutes), 20% to 60% (5.01–25 minutes), 60% to 100% (25–26 minutes), 100% (26–30 minutes), 100% to 0% (30–31 minutes), and 0% (31–40 minutes). The flow rate was 0.5 mL/min, the injection volume was 20 μL, and the detection was performed simultaneously at five wavelengths: 254, 280, 360, 390, and 450 nm for GSH-KN, AHA, and KN and 254, 280, 372, 390, and 450 nm for 3OHKN and 3OHKG. The chromatograms were recorded and the peak areas integrated (ChemStation for Windows; Agilent).

Semipreparative HPLC was used for the separation of newly synthesized UV filters (GSH-KN, 3OHKG, and AHA) and was performed on a 16 × 250-mm, 7-μm C16 preparative column (Diasorb-

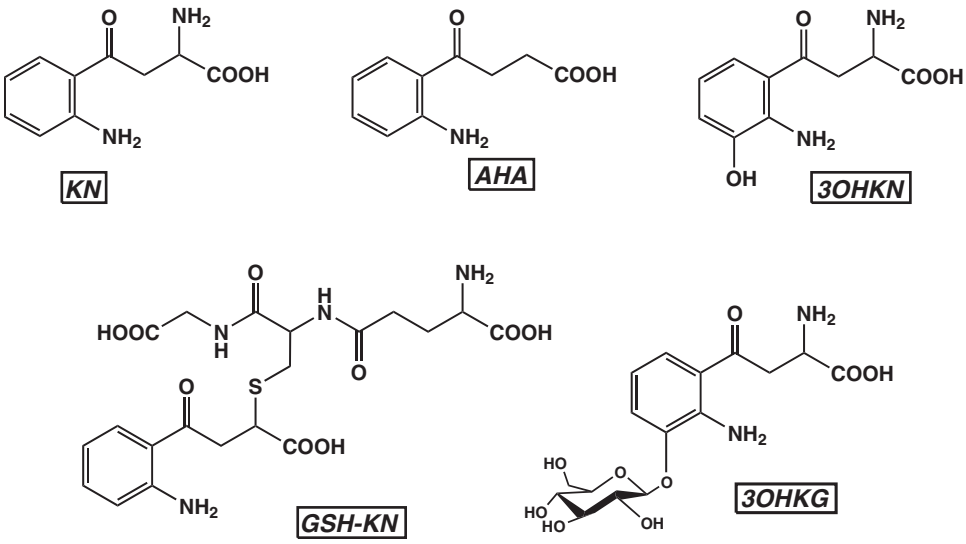

CHART 1. Structures of the UV filter molecules.

130-C16-TX; BioChimMac, Moscow, Russia) using an acetonitrile/0.05% (vol/vol) TFA in H_2O gradient. The acetonitrile percentage in the gradient for GSH-KN and 3OHKG was 0% (0–5 minutes), 0% to 50% (5–25 minutes), 50% to 100% (25–26 minutes), 100% (26–30 minutes), 100% to 0% (30–31 minutes), and 0% (31–40 minutes) and for AHA, 0% (0–5 minutes), 0% to 20% (5–5.01 minutes), 20% to 80% (5.01–25 minutes), 80% to 100% (25–26 minutes), 100% (26–30 minutes), 100% to 0% (30–31 minutes), and 0% (31–40 minutes). The flow rate was 5.0 mL/min, the injection volume was 1 mL, and the detection was performed simultaneously at the same wavelengths as mentioned above.

The purification of commercially available compounds (KN and 3OHKN) was performed on a 16 × 250-mm, 7-μm preparative column (Diasorb-130-C16-TX; BioChimMac), using acetonitrile/0.05% (vol/vol) TFA in H_2O gradient. The acetonitrile percentage in the gradient was 0% (0–5 minutes), 0% to 20% (5–6 minutes), 20% to 60% (6–25 minutes), 100% (25–30 minutes), 0% (30–30.01 min), 0% (30.01–40 minutes). The flow rate was 5 mL/min, the injection volume was 1 mL, and the detection was performed simultaneously at five wavelengths: 280, 360, 372, 400, and 480 nm.

Steady State Absorption and Fluorescence

Absorption spectra were recorded with spectrophotometers (Agilent 8453; Hewlett-Packard, La Jolla, CA, and Cary 50; Varian, Palo Alto, CA); fluorescence spectra were measured with a fluorometer (Cary Eclipse; Varian). All fluorescence spectra were corrected for the wavelength-dependent sensitivity of the detection. For all measurements, a 10 × 10-mm^2 quartz cell was used, and the absorbance of the samples was below 0.1 at the absorption maximum.

Femtosecond-Resolved Fluorescence

The fluorescence dynamics was measured using the fluorescence upconversion setup described in detail elsewhere.[29] Briefly, part of the output of a tunable mode-locked Ti:Sapphire laser (MaiTai; Spectra Physics-Newport Corp., Irvine, CA) was frequency doubled and used to excite the sample at 390 nm. The polarization of the probe pulses was at the magic angle relative to that of the gate pulses at 780 nm. The fluorescence was gated by sum-frequency mixing with the fundamental of the oscillator output. The upconverted UV photons were directed into a monochromator and detected by a photomultiplier tube with photon-counting electronics. The sample solutions were kept in a 1.0-mm-thick spinning cell and they had an absorbance of ~0.2 at the excitation wavelength. The full width at half-maximum (FWHM) of the instrument response function was ~210 fs.

Femtosecond-Resolved Pump-Probe Transient Absorption (TA)

The experimental setup has been described in detail elsewhere.[30,31] Excitation was performed at 400 nm, using the frequency-doubled output of a standard 1-kHz amplified Ti:Sapphire system (Spectra Physics-Newport Corp.). The pump intensity on the sample was ~1.5 mJ/cm^2. Probing was achieved with a white-light continuum obtained by focusing a small fraction of the 800-nm pulses in a CaF_2 plate. The polarization of the probe pulses was at the magic angle relative to that of the pump pulses. All spectra were corrected for the chirp of the white-light probe pulses. The FWHM of the instrument response function was ~200 fs. The sample solutions were placed in a 1-mm-thick quartz cell where they were continuously stirred by N_2-bubbling. Their absorbance at the excitation wavelength was ~0.2.

Laser Flash Photolysis (LFP)

Our LFP setup is described elsewhere[32,33] and has recently been upgraded. Briefly, solutions, placed in a rectangular cell (inner dimensions 10 mm × 10 mm), were irradiated with either an Nd:YAG laser (pulse duration 8 ns; 532 nm: pulse energy up to 225 mJ; 355 nm: pulse energy up to 135 mJ; and 266 nm: pulse energy up to 65 mJ Quanta-Ray LAB-130-10; Newport Corp.) or an excimer laser (pulse duration, 15–20 ns; 308 nm: pulse energy up to 100 mJ; Lambda Physik EMG 101; Coherent, Inc., Santa Clara, CA;). In the present work, only the excimer laser was used. A fraction of the laser beam was split by a quartz plate and directed to a photodiode for triggering the oscilloscope and to a power meter (1918-C; Newport Corp.) for the permanent monitoring of the laser energy. The dimensions of the laser beam at the front of the cell were 2.5 mm × 8 mm. The monitoring system includes a xenon short-arc lamp (model DKSh-150, Stella ltd., Moscow, RF) connected to a high-current pulser, a monochromator (78025; Newport Corp.), a photomultiplier (9794B; ET Enterprises, Ltd., Uxbridge, UK), and a digital oscilloscope (WaveRunner 104MXi; LeCroy, Chestnut Ridge, NY). The monitoring light, concentrated in a rectangular of 2.5-mm height and 1-mm width, passed through the cell along the front (laser irradiated) window. Thus, in all experiments the excitation optical length was 1 mm, and the monitoring optical length was 8 mm. All peripheral devices (lasers, shutters, monochromator, power meter, and digitizer) were computer controlled. All solutions were bubbled with argon for 10 minutes before and during irradiation.

Steady State Photolysis

The solutions for steady state photolysis were prepared in a phosphate buffer (pH 7.0), the UV filter concentrations (near 0.7 mM) were adjusted in such a way that all solutions had the same absorbance of A = 3.0 at the absorption maxima for a 1-cm optical path. The samples were placed in NMR glass tubes (5 mm outer diameter) and irradiated with a mercury lamp (model 1000; DKSH). The sample volume was 1 cm^3. A water filter cut off infrared light. The wavelength region from 300 to 400 nm was selected with a set of ultraviolet glass filters. The solutions were bubbled with argon for 10 minutes before and during irradiation. During the irradiation, samples (16 μL) were periodically taken off the solution by a syringe and stored at −20°C until use. These samples were diluted with water up to 200 μL and analyzed by HPLC.

Actinometry was performed with an aqueous solution of potassium ferrioxalate, according to standard methods.[34] The light intensity at the sample in the 300 to 400 nm region was equal to $(1.9 \pm 0.2) \times 10^{18}$ quanta per second.

Quantum Chemical Calculations

Ground-state gas-phase geometry optimization was performed at the density functional theory (DFT) level, using the B3LYP functional[35] and a [3s2p1d] basis set.[36] Electronic vertical excitation energies were computed with time-dependent density functional theory (TD-DFT) using the same functional and basis set.[37] The calculations were performed using Turbomole version 6.0.[38]

Results

Steady State Measurements

The absorption and emission spectra of the studied UV filters were measured in aqueous-buffered solution (phosphate-buffered saline, PBS [pH 7.4]). The spectra of all UV filters are similar with an absorption maximum near 360 nm and an emission maximum near 490 nm (Fig. 1). The exceptions are 3OHKN and 3OHKG, for which both absorption and fluorescence maxima are red-shifted to ~370 and ~550 nm for 3OHKN, and to ~365 and ~505 nm for 3OHKG, respectively. This shift can be attributed to the presence of the oxygen substituent on the phenyl ring. The smaller shifts observed with 3OHKG can be explained by the glycoside moiety that reduces the influence of the oxygen on the aromatic system.

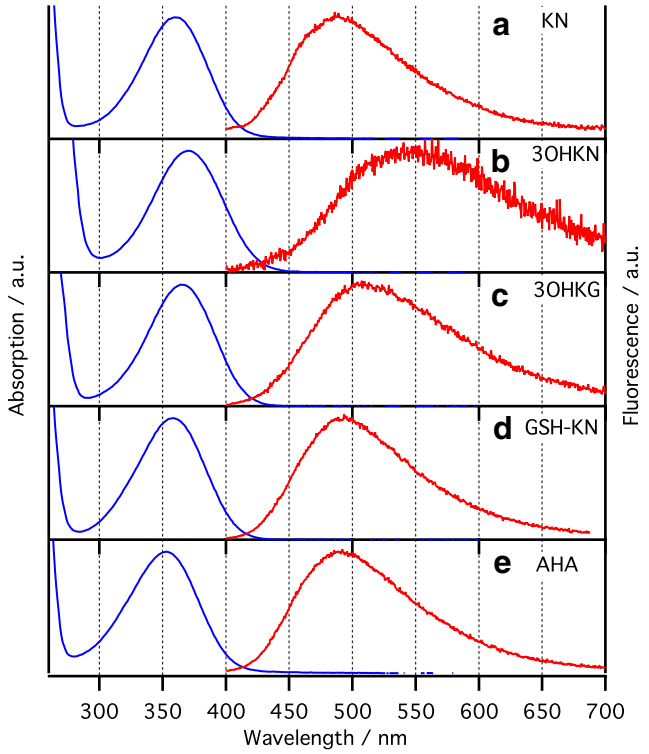

Figure 1. Absorption (*blue traces*) and emission (390 nm excitation, *red traces*) spectra of the UV filters in PBS solution.

The fluorescence quantum yields of the UV filters, Φ_F, measured relative to quinine bisulfate ($\Phi_F = 0.55$),[39] are listed in Table 1. The values for KN, 3OHKN, and GSH-KN are in a good agreement with those published earlier.[21,24]

Time-Resolved Fluorescence Measurements

Fluorescence time profiles of the UV filters in PBS were recorded after 390-nm excitation and 540 nm detection at a magic angle over different time windows up to 500 ps. The normalized time profiles within the first 200 ps are shown in Figure 2. Except for 3OHKN, all UV filters exhibit an initial increase lasting some picoseconds, followed by a monotonic decay (Fig. 2, inset). The rising signal is due to solvent relaxation, which leads to a dynamic Stokes shift of the fluorescence spectrum. According to our previous studies of KN and its adducts, the solvent relaxation of KNs predominantly occurs in two stages: (1) diffusive motion of the solvent molecules around the excited UV filter molecule, typically ~1 ps in aqueous solution and (2) conformational changes of UV filter

Table 1. Parameters of the UV Filters

UV Filter	τ_S/ps*	$\Phi_{fl} \times 10^4$	$\Phi_T \times 10^3$	$\Phi_{dec} \times 10^5$
KN	26.9 ± 0.8	9.2 ± 1.0	7.0 ± 1.7	1.5 ± 0.2
3OHKN	10.2 ± 1.2	1.3 ± 0.2	—	4.4 ± 0.3
3OHKG	29.3 ± 0.5	6.9 ± 0.6	6.3 ± 1.5	3.4 ± 0.5
KN-GSH	48.1 ± 2.7	13 ± 2	11 ± 3	6.2 ± 0.7
AHA	44.2 ± 2.1	14 ± 2	12 ± 3	2.9 ± 0.4

Singlet-excited state lifetime (τ_S), fluorescence quantum yield (Φ_{fl}), triplet quantum yield (Φ_T), and quantum yield of the anaerobic photodecomposition (Φ_{dec}) of the UV filters in aqueous-neutral solutions.

* Average of the lifetime obtained by time-resolved fluorescence and TA.

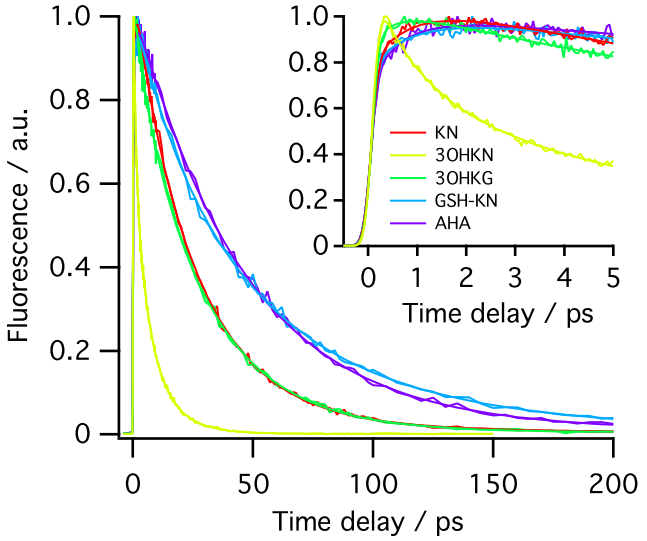

Figure 2. Time profiles of the fluorescence intensity (390 nm excitation) measured at 540 nm in PBS solutions (pH 7.4) of KN (*red trace*), 3OHKN (*yellow trace*), 3OHKG (*green trace*), GSH-KN (*blue trace*) and AHA (*purple trace*) and best multiexponential fits. *Inset*: early fluorescence dynamics.

geometry in the excited state, approximately 4 to 10 ps, depending on the substituent.[21,24] The time resolution of the experiment is not sufficient for the inertial part of solvation, that takes place in ≤100 fs, to be resolved. In the case of 3OHKN, the solvent relaxation is hidden by the fast decay of the excited state population.

The obtained data were analyzed using the sum of four exponential functions convolved with the Gaussian-like instrument response function. The best fits are presented as smooth lines in Figure 2, and the time constants and amplitudes are listed in Table 2 (the sum of amplitudes was normalized to unity). The first two components can be attributed to the relaxation dynamics in the excited state as mentioned above, and the third component to the S_1 state lifetime. The last exponential function was added for a proper description of the fluorescence from impurities and products formed during the measurements (the amplitude of this component was small for all UV filters; Table 2). For 3OHKN, good agreement between experimental data and calculations was achieved, using three exponential functions.

Table 2. Characteristic Time Constants (τ_i, i = 1,2,3,4) of the Excited-State Dynamics of the UV Filters in PBS Solution (pH 7.4)

	τ_1/ps	τ_2/ps	τ_3/ps	τ_4/ps
KN	0.8 (−0.39)*	5.4 (0.09)*	26.3 (1.27)*	120 (0.03)*
	1.0†	4.7†	27.4†	
3OHKN	1.0 (0.39)*	5.4 (0.37)*	11.1 (0.24)*	
	0.7†	—	9.2†	
AHA	0.6 (−0.41)*	4.1 (−0.07)*	45.7 (1.47)*	940 (0.01)*
	1.4†	13.6†	42.7†	
KN-GSH	0.9 (−0.31)*	16.9 (0.23)*	50.0 (1.03)*	140 (0.05)*
	1.1†	8.5†	46.2†	
3OHKG	0.4 (−0.19)*	5.2 (0.15)*	29.0 (1.03)*	360 (0.007)*
	0.9†	5.8†	29.7†	

Relative amplitudes are in parentheses.

* Measured by fluorescence upconversion (λ_{ex} = 390 nm).

† Measured by TA (λ_{ex} = 400 nm).

Femtosecond TA Measurements

The TA spectra of the UV filters in PBS solution were recorded after 400 nm excitation. Selected spectra are presented in Figures 3 A1–E1 for KN, 3OHKN, 3OHKG, GSH-KN, and AHA, respectively. In all spectra, the main positive TA band exhibited a blue shift followed by a monotonic decay. As discussed earlier,[21,24] the observed TA bands are a superposition of $S_1 \rightarrow S_n$ absorption and $S_1 \rightarrow S_0$ stimulated emission bands, the latter being the origin of a negative feature around 600 nm. The observed blue shift is due to a solvent-induced red shift of the stimulated emission band and, probably, a blue shift of the $S_1 \rightarrow S_n$ absorption band.[21,24]

The TA spectra were analyzed globally using the sum of three exponential functions and an offset value y_0, accounting for the signal arising from minor long-lived impurities present in the solution and/or products formed during the measurements. Only two exponential functions were necessary to reproduce the evolution of TA spectra measured with 3OHKN. The obtained time constants are listed in Table 2, and the decay associated spectra (DAS), $A_1(\lambda)$, $A_2(\lambda)$, and $A_3(\lambda)$ are displayed in Figure 3. For all UV filters, the fast components $A_1(\lambda)$ and $A_2(\lambda)$ exhibit similar shapes with positive and negative bands, indicating a decay on the low-energy side of the spectrum and a rise on the high-energy side of the spectrum. These components can thus be attributed to a dynamic Stokes shift, in full agreement with our previous investigations.[21,24] The third component corresponds to the S_1 state lifetime with a characteristic time constants τ_3 similar to the values obtained in the fluorescence measurements. In the case of 3OHKN, the second component of the solvation dynamics was not properly resolved, because of the fast decay of the S_1 state population; the $A_1(\lambda)$ spectrum should be assigned to a cumulative Stokes shift dynamics and the $A_2(\lambda)$ spectrum to the decay of excited state population, the corresponding time constants being listed as τ_1 and τ_3 in Table 2. In Table 1, the S_1 state lifetimes of the photoexcited UV filters are given as average values of the time constants obtained in time-resolved fluorescence and TA measurements.

Nanosecond Laser Flash Photolysis: Triplet Quantum Yield Measurements

The measurements of the triplet quantum yield were performed by comparing the results of direct and acetone-sensitized photolysis under anaerobic conditions. The sample for the direct photolysis contained 9.5×10^{-4} M KN and 1.2×10^{-2} M acetone in phosphate buffer (pH 6.9). Acetone was added to the solution as an electron scavenger to prevent the formation of kynurenine electron adduct KNH$^{\cdot}$, which can be generated in the solution due to biphotonic ionization of KN followed by electron addition to KN ground state.[17] In this solution, the absorbance of KN at 308 nm in the 1 cm cell was $A_{KN} = 0.85$, and that of acetone was $A_{Ac} = 7.3 \times 10^{-3}$ (i.e., most of the incident light was absorbed by KN). For convenience, this solution will be called low-acetone (LA) samples. The second sample (high-acetone HA samples), prepared for the sensitized photolysis, contained 2.2×10^{-4} M KN ($A_{KN} = 0.20$) and 1.39 M acetone ($A_{Ac} = 0.85$)—that is, the absorbance of acetone was much higher than that of KN in this sample, and this absorbance is equal to the absorbance of KN in the LA sample. The samples were irradiated by 308-nm laser pulses, and the transient absorption was measured at 430 nm (absorption maximum of the KN triplet state[16,17]). The general scheme of the reactions occurring under 308-nm laser irradiation of the sample, containing mixture of KN and acetone, is the following:

$$\mathrm{Ac} \xrightarrow{h\nu,\ \mathrm{ISC}} {}^3\mathrm{Ac} \qquad (1)$$

$$\mathrm{KN} \xrightarrow{h\nu,\ \mathrm{ISC}} {}^3\mathrm{KN} \qquad (2)$$

$${}^3\mathrm{Ac} + {}^3\mathrm{Ac} \rightarrow \mathrm{Ac} + {}^1\mathrm{Ac}^* \qquad (3)$$

$${}^3\mathrm{Ac} + \mathrm{KN} \xrightarrow{k_1} \mathrm{Ac} + {}^3\mathrm{KN} \qquad (4)$$

$${}^3\mathrm{KN} + {}^3\mathrm{KN} \xrightarrow{k_2} \mathrm{KN} + {}^1\mathrm{KN}^* \qquad (5)$$

Reaction 2 can be ignored in the photolysis of the HA samples. At low laser energies (i.e., at low triplet ^{3}Ac concentrations) and sufficiently high KN concentrations, reaction 3 can also be ignored, and reaction 5 is slow compared to reaction 4. A kinetic trace obtained under such experimental conditions (laser energy 0.32 mJ) is shown in Figure 4, trace 1. This trace can be reproduced with a biexponential function:

$$\Delta A_{sens} = A[\exp(-k_1 t) - \exp(-k_2 t)] \qquad (6)$$

where the larger rate constant corresponds to the population of the triplet state of KN (reaction 4), the smaller one to the decay of the triplet state population (reaction 5), and the value A to the absorption of the total amount of ^{3}KN formed in the reaction. The approximation of the second-order reaction 5 by the exponential function does not lead to a significant error, since only the initial part of the kinetic trace is taken into account.

In the photolysis of LA samples, the absorption of KN at 308 nm is two orders of magnitude greater than that of acetone. Nevertheless, one can see that the formation of the triplet KN by direct photolysis (ΔA observed immediately after the laser pulse; Fig. 4, trace 2) is comparable with that due to the acetone-sensitized photolysis (signal growth from 0 to 1 μs). Apparently, this observation should be attributed to the low triplet quantum yield of the direct KN photolysis, whereas the efficiency of the acetone-sensitized photolysis under experimental conditions is close to 100%. The kinetic traces obtained in the photolysis of the LA samples were analyzed using the following function:

$$\Delta A_{dir} = B \times \exp(-k_1 t) - C \times \exp(-k_2 t) \qquad (7)$$

where the value $(B - C)$—in other words, the initial transient absorption observed immediately after the laser pulse—was attributable to the absorption of ^{3}KN formed by direct photolysis (reaction 2). The triplet quantum yield in the direct KN photolysis, Φ_T, was determined presuming a 100% efficiency of the acetone-sensitized photolysis:

$$\Phi_T = \frac{B - C}{A} \times \frac{E_{LA}}{E_{HA}} \qquad (8)$$

Here E_{LA} and E_{HA} are the laser energies used in the photolysis of the LA and HA samples. The measurements were performed

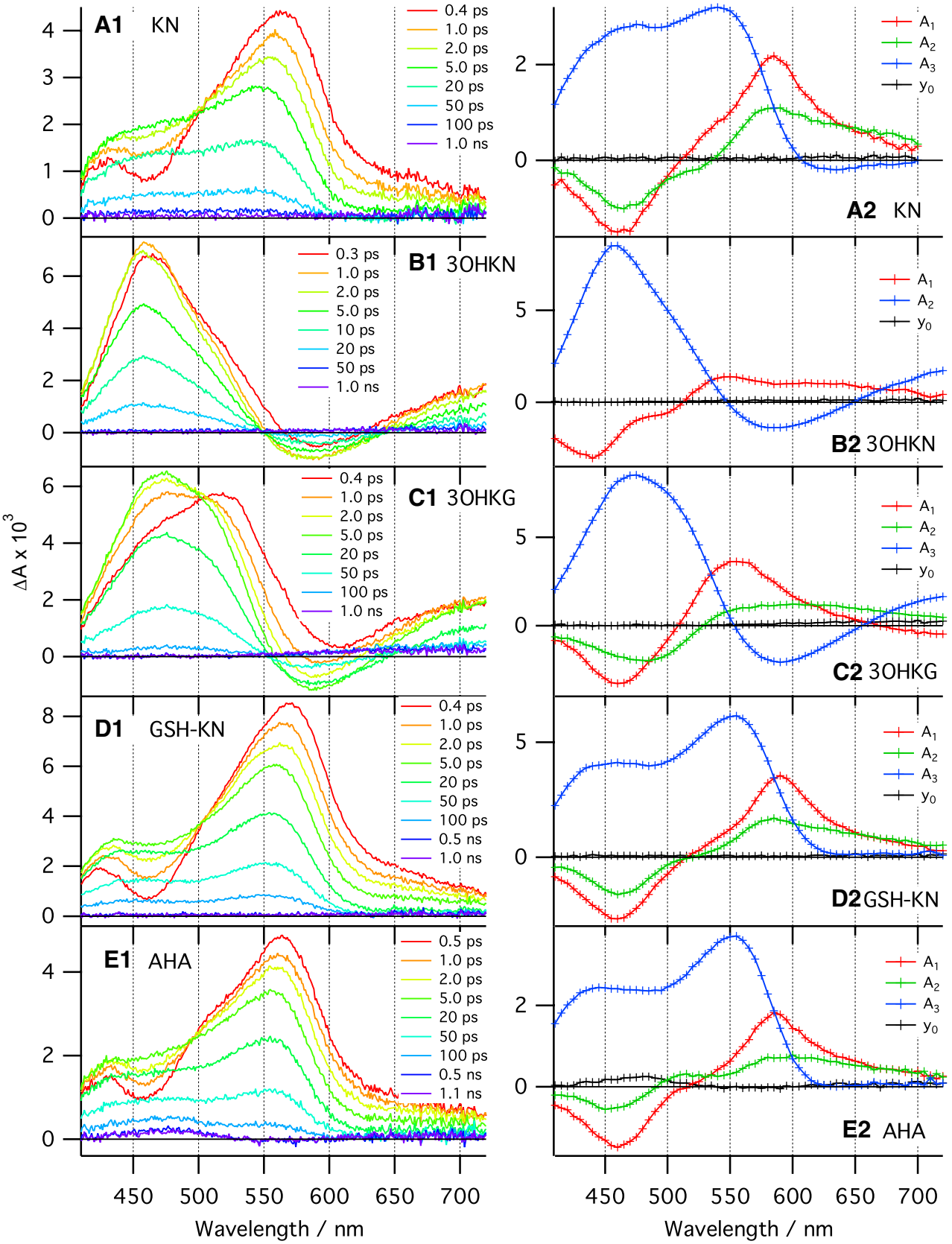

Figure 3. TA spectra (**A1–E1**) recorded at different time delays after 400 nm excitation of PBS solutions of the UV filters and decay associated spectra (**A2–E2**) obtained from a global analysis of the TA spectra. The components A_1, A_2, and A_3 correspond to exponential functions with the characteristic time constants τ_1, τ_2, and τ_3 (Table 2), and the offset value y_0 corresponds to the time-independent component of kinetics.

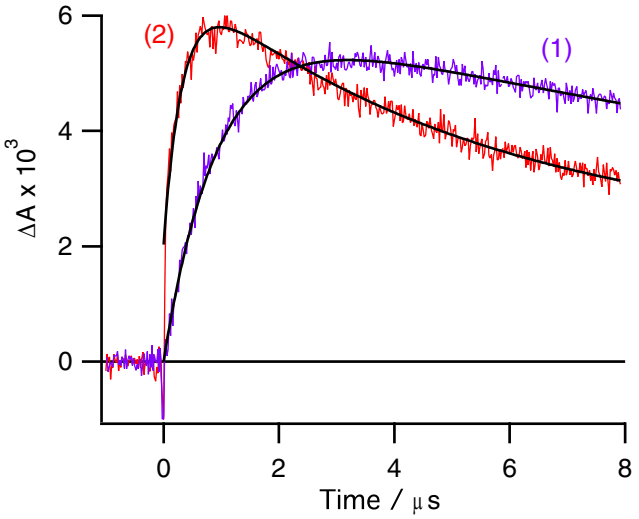

FIGURE 4. TA profiles recorded after 308-nm excitation of (trace 1) HA sample, laser energy 0.32 mJ/pulse, and (trace 2) LA sample, laser energy 9.8 mJ/pulse. *Black lines*: best biexponential fit (equations 6 and 7).

with several laser energies ranging from 0.32 to 3.4 mJ (for HA samples) and from 6.2 to 40 mJ (for LA samples). For both types of samples, linear dependences of A versus E_{HA} and $(B - C)$ versus E_{LA} were observed. The average value of the triplet yield was found to amount to $\Phi_T = (7.0 \pm 1.7) \times 10^{-3}$.

The triplet quantum yields of the other UV filters were measured in a similar way, with the exception of 3OHKN, whose triplet absorption above 400 nm is too low for a reliable detection[17] and which overlaps with the absorption of the starting compound at shorter wavelengths. These results are summarized in Table 1.

Photodecomposition Quantum Yield

Figure 5 shows the kinetics of UV filter decomposition measured on exposing the deaerated samples to continuous UV irradiation. During the initial period of irradiation, all samples exhibited a linear decay of the concentration versus time. When the UV filter concentration decayed below 50%, the photodecomposition rate decreased. This can be accounted for by two effects: the decrease of the starting compound absorption and the increase of the photoproduct absorption. Thus, the calculations of the photodecomposition quantum yield Φ_{dec} were performed with the linear part of the kinetic curves only (Fig. 5, straight lines). The Φ_{dec} values were calculated as the ratio of the total quantity of the UV filter molecules converted into photoproducts over a period to the quantity of the light quanta absorbed by the sample over the same period (Table 1).

Discussion

The initial step of most photochemical reactions is the population of the first singlet excited state of a molecule, either on direct $S_1 \leftarrow S_0$ excitation or after $S_{n>1} \leftarrow S_0$ excitation and subsequent internal conversion. The main decay pathways of the S_1 state population are internal conversion (IC) and fluorescence to the ground state, and intersystem crossing (ISC) into the triplet state. IC is the most desirable decay pathway of the S_1 state of the UV filters contained in the lens: the absorbed light energy is transferred to heat without damaging the absorber or the surrounding molecules. Fluorescence is an undesirable process as one does not need extra light inside the eye. ISC is a harmful channel because molecules in the triplet state are relatively long-lived and reactive species, which can react with other molecules inside the lens.

As demonstrated in earlier publications[21,24] and in this work, the main decay channel of the UV filter S_1 states in aqueous solutions is a very fast hydrogen-bond–assisted IC,[21] which accounts for more than 99% of all absorbed light quanta. Thus, the excited singlet lifetime τ_S and the triplet yield Φ_T are closely connected quantities determining the "quality" of UV filters: an absorber with the shorter τ_S produces fewer triplet molecules, and, consequently, is less photoactive and more photostable. Indeed, Table 1 reveals an obvious correlation between the τ_S and Φ_T values: the primary UV filters KN, 3OHKN, and 3OHKG are characterized by shorter singlet lifetimes and smaller triplet quantum yields than the secondary filters AHA and GSH-KN.

The difference between KN, 3OHKN, and AHA is apparently connected with the presence of the hydroxyl group in 3OHKN and the absence of the amino group in AHA. For a better understanding of the influence of these substituents on the photophysics of KN and related compounds, quantum chemistry calculations at the DFT level have been performed with KN, 3OHKN, and AHA. For KN and 3OHKN, the calculations were done starting with the zwitterionic form (i.e., the protonated amino group and deprotonated carboxylic group). However, the gas-phase geometry optimization resulted in both cases to the neutral form as the most stable one; the same effect for KN was recently reported.[40] Clearly, water is needed to stabilize the zwitterionic form. However, calculations with water are quite demanding because of the occurrence of H bonds, whereas the gas-phase results yield a qualitative explanation for the differences in the excited-state lifetime.

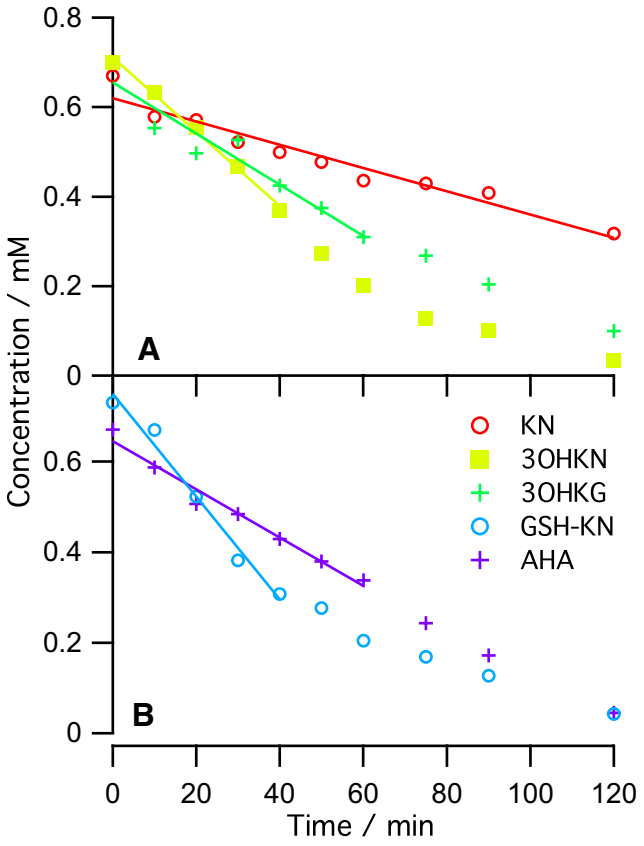

FIGURE 5. Kinetics of anaerobic UV filter decomposition with a UV light intensity of 1.9×10^{18} quanta/s and linear fits. Data were obtained from the integration of HPLC profiles of irradiated samples.

TD-DFT calculations with KN predict the first transition at 328 nm with a dipole moment of 2.5 D. This blue shift relative to the observation could be accounted for by the lack of solvation shell. This transition is associated with a one-electron HOMO-LUMO transition. Figure 6 shows that this transition is associated with a decrease in the electron density on the aromatic amino group and an increase on the carbonyl group. This confirms the charge transfer (CT) character of this transition and the strengthening of the H-bond on the carbonyl group in the excited state.

Very similar results were obtained with 3OHKN. The first transition, predicted at 333 nm (2.5 D), involves a one-electron HOMO-LUMO transition as well. Figure 6 shows that the electronic density at the aromatic OH group decreases on excitation. The hydroxyl group seems thus to somewhat increase the CT character of this transition compared with KN. Indeed, the difference of electronic density on the carbonyl oxygen between HOMO and LUMO seems slightly larger for 3OHKN than for KN (the density on the oxygen is smaller on the HOMO of 3OHKN than on the HOMO of KN). This small difference could lead to slightly stronger H-bonds with the solvent and thus might account for the shorter excited-state lifetime of 3OHKN.

The results obtained for AHA were quite different. The first transition predicted at 313 nm with a dipole moment of 2.1 D is described by a combination of HOMO-LUMO (65%) and HOMO-1-LUMO (27%) transitions (Fig. 6). Whereas the first transitions of KN and 3OHKN are pure HOMO-LUMO CT transitions, this transition in AHA has intrinsically less CT character because of a substantial contribution from the HOMO-1-LUMO transition, which is instead an $n\pi^*$ transition. Because of this smaller CT character, the H-bonds between AHA in the S_1 state and the solvent molecules should be weaker than for KN and 3OHKN.

These calculations appear to give some rationale to the decreasing excited state lifetime observed by going from AHA to KN and to 3OHKN. This trend correlates well with the increase of electronic density on the carbonyl oxygen on photoexcitation, which is the driving force for the fast hydrogen bond-assisted IC. The increase of electronic density on the carbonyl oxygen is the weakest with AHA because the transition is not a pure $\pi\pi^*$ with a high CT character but possesses some $n\pi^*$ character. On the other hand, it is the strongest in 3OHKN because of the presence of the hydroxyl group.

The relatively long S_1 state lifetime of GSH-KN probably has a steric rather than an electronic origin. It has recently been shown[24] that all adducts of KN to amino acids have noticeably longer S_1 lifetimes than KN itself. The bulky substituent near the carbonyl group most likely partially blocks its exposure to the solvent molecules, and, as a consequence, weakens intermolecular hydrogen bonds. As a result, the efficiency of the solvent-assisted IC decreases, and the S_1 state lifetime increases.

The values of the fluorescence quantum yield correlate well with the singlet lifetimes: the secondary UV filters AHA and GSH-KN produces stronger fluorescence than KN, 3OHKN, and 3OHKG. We should notice however that the fluorescence of all compounds under study is rather low, and the presence of even small amounts of fluorescent impurities can introduce a significant error in the fluorescence quantum yield measurements. Thus, the obtained Φ_{fl} values should only be considered as indirect manifestations of the UV filter qualities.

The triplet quantum yield value $\Phi_T = (7.0 \pm 1.7)\times10^{-3}$, obtained here for KN, is more than twice lower than the value $\Phi_T = 0.018 \pm 0.004$ published by one of our groups 6 years ago.[16] Inspection of the previous data revealed that a major source of error[16] was the neglect of the contribution of biphotonic processes in the direct KN photolysis. Indeed, the measurements were performed at relatively high laser energies, without the addition of the electron scavenger acetone. As a result, the electron adduct of KN was formed due to the

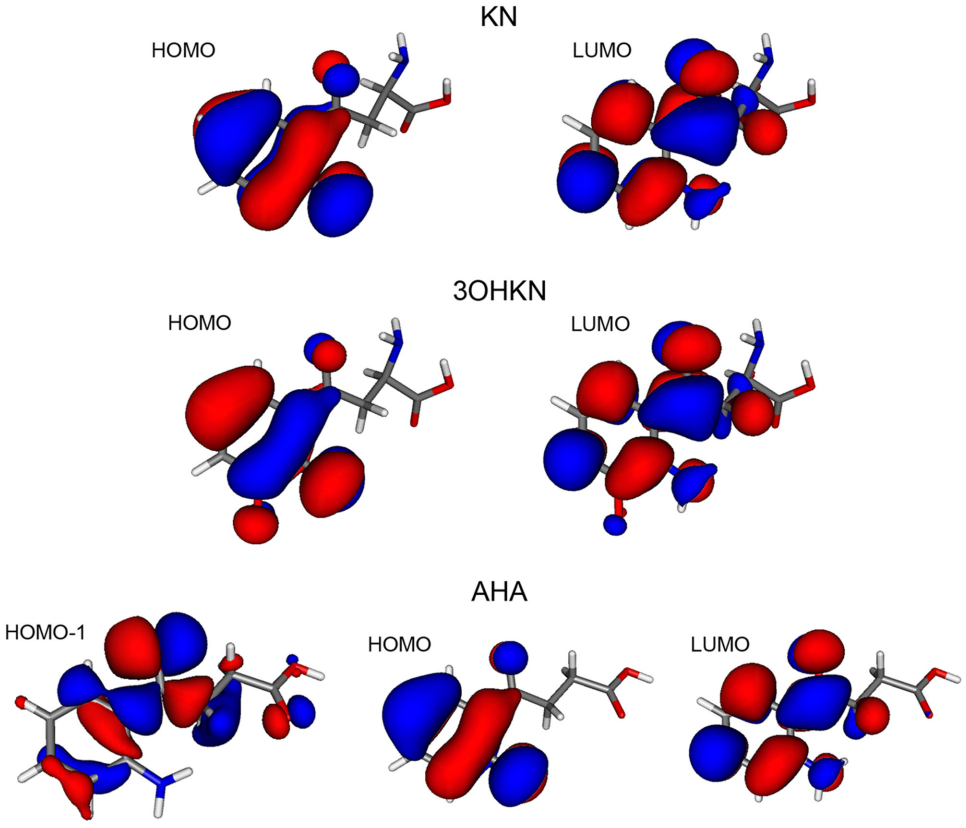

Figure 6. Frontier molecular orbitals of KN, 3OHKN, and AHA drawn at the 0.02 AU level. The calculations were performed at the density functional theory level (DFT), using the B3LYP functional and a [3s2p1d] basis set.

biphotonic ionization of KN followed by the addition of the solvated electron to KN in the ground state. This gave a substantial contribution to the observed absorption at 430 nm. Thus, the previously published value for Φ_T was overestimated.

The photodecomposition quantum yield is a generic parameter, which depends not only on the photochemical properties of the parent compound, but also on the properties of photoproducts, which can absorb UV light and facilitate the decomposition of the starting material. That is most likely the case for 3OHKN, because among all the UV filters studied here, it has the shortest S_1 lifetime, and yet its decomposition yield is almost three times as high as that of KN. Indeed, under irradiation, a 3OHKN solution rapidly turns yellow.

The difference in the photoactivity of the UV filters can be very important for the susceptibility of the human eye to UV irradiation. In young human lenses, the concentration of the most abundant UV filter, 3OHKG, varies between 300 and 600 nmoles/g, whereas in 80-year-old lenses, the level of 3OHKG decreases to 30 to 150 nmoles/g.[5] At the same time, the GSH-3OHKG content, which is near the detectable level in the young lenses, rises to 30 to 120 nmoles/g in 80-year-old lenses.[5] The AHBG level does not change significantly with age, being 20 and 80 nmoles/g in young lenses and 10 to 50 nmoles/g in old ones.[5] Altogether, the primary/secondary UV filters ratio can be estimated as approximately 10:1 in young human lenses, whereas in old lenses it falls to approximately 2:1. As we demonstrate here, the quality of the secondary UV filters is inferior compared to primary ones, which makes the old lenses more susceptible to UV light. Beside this, old lenses contain a significant amount of UV filters covalently linked to the lens proteins,[26,41–43] and the quality of kynurenines bound to proteins are much worse than that of the free UV filters (i.e., the singlet lifetimes are longer, and the fluorescence and triplet quantum yields are higher).[24,44,45] Apparently, in a complex biological system that is the human lens many other factors can influence the susceptibility to UV light—in particular, the coloration of the lens proteins due to posttranslational modifications and the abundance of antioxidants which can deactivate photoexcited molecules. Nevertheless, our results indicate that the UV protection of old lenses is weaker than that of young ones, which might be an important factor for the development of the age-related cataract.

References

1. van Heyningen R. Fluorescent glucoside in the human lens. *Nature.* 1971;230:393–394.
2. Wood AM, Truscott RJW. UV filters in human lenses: tryptophan catabolism. *Exp Eye Res.* 1993;56:317–325.
3. Wood AM, Truscott RJW. Ultraviolet filter compounds in human lenses: 3-hydroxykynurenine glucoside formation. *Vis Res.* 1994; 34:1369–1374.
4. Truscott RJW, Wood AM, Carver JA, et al. A new UV-filter compound in human lenses. *FEBS Lett.* 1994;384:173–176.
5. Bova LM, Sweeney MH, Jamie JF, Truscott RJW. Major changes in human ocular UV protection with age. *Invest Ophthalmol Vis Sci.* 2001;42:200–205.
6. Streete IM, Jamie JF, Truscott RJW. Lenticular levels of amino acids and free UV filters differ significantly between normals and cataract patients. *Invest Ophthalmol Vis Sci.* 2004;45:4091–4097.
7. Mizdrak J, Hains PG, Kalinowski D, Truscott RJW, Davies MJ, Jamie JF. Novel human lens metabolites from normal and cataractous human lenses. *Tetrahedron.* 2007;63:4990–4999.
8. Snytnikova OA, Fursova AZ, Chernyak EI, et al. Deaminated UV filter 3-hydroxykynurenine O-β-D-glucoside is found in cataractous human lenses. *Exp Eye Res.* 2008;86:951–956.
9. Moroni F. Tryptophan metabolism and brain function: focus on kynurenine and other indole metabolites. *Eur J Pharm.* 1999;375: 87–100.
10. Taylor LM, Aquilina JA, Jamie JF, Truscott RJW. UV filter instability: consequences for the human lens. *Exp Eye Res.* 2002;75:165–175.
11. Tsentalovich YP, Snytnikova OA, Forbes MDE, Chernyak EI, Morozov SV. Photochemical and thermal reactivity of kynurenine. *Exp Eye Res.* 2006;83:1439–1445.
12. Taylor LM, Aquilina JA, Jamie JF, Truscott RJW. Glutathione and NADH, but not ascorbate, protect lens proteins from modification by UV filters. *Exp Eye Res.* 2002;74:503–511.
13. Kopylova LV, Snytnikova OA, Chernyak EI, Morozov SV, Tsentalovich YP. UV filter decomposition: a study of reactions 4-(2-aminophenyl)-4-oxocrotonic acid with amino acids and antioxidants present in the human lens. *Exp Eye Res.* 2007;85:242–249.
14. Krishna CM, Uppuluri S, Riesz P, Zigler JS, Balasubramanian D. A study of the photodynamic efficiencies of some eye lens constituents. *Photochem Photobiol.* 1991;54:51–58.
15. Reszka KJ, Bilski P, Chignell CF, Dillon J. Free radical reactions photosensitized by the human lens component, kynurenine: an EPR and spin trapping investigation. *Free Radical Biol Med.* 1996; 20:23–34.
16. Tsentalovich YP, Snytnikova OA, Sherin PS, Forbes MDE. Photochemistry of kynurenine, a tryptophan metabolite: properties of the triplet state. *J Phys Chem A.* 2005;109:3565–3568.
17. Snytnikova OA, Sherin PS, Tsentalovich YP. Biphotonic ionization of kynurenine and 3-hydroxykynurenine. *J Photochem Photobiol A Chem.* 2007;186:364–368.
18. Snytnikova OA, Sherin PS, Kopylova LV, Tsentalovich YP. Kinetics and mechanism of reactions of photoexcited kynurenine with molecules of some natural compounds. *Russ Chem Bull.* 2007;56: 732–738.
19. Sherin PS, Tsentalovich YP, Snytnikova OA, Sagdeev RZ. Photoactivity of kynurenine-derived UV filters. *J Photochem Photobiol B Biol.* 2008;93:127–132.
20. Tsentalovich YP, Snytnikova OA, Sagdeev RZ. Photochemical and thermal reactions of kynurenines. *Russ Chem Rev.* 2008;77:789–797.
21. Sherin PS, Grilj J, Tsentalovich YP, Vauthey E. Ultrafast excited-state dynamics of kynurenine: a UV filter of the human eye. *J Phys Chem B.* 2009;113:4953–4962.
22. Dillon J, Wang RH, Atherton SJ. Photochemical and photophysical studies on human lens constituents. *Photochem Photobiol.* 1990; 52:849–854.
23. Ervin LA, Dillon J, Gaillard ER. Photochemically modified α-crystallin: a model system for aging in the primate lens. *Photochem Photobiol.* 2001;73:685–691.
24. Sherin PS, Grilj J, Kopylova LV, Yanshole VV, Tsentalovich YP, Vauthey E. Photophysics and photochemistry of UV filter kynurenine covalently attached to amino acids and to a model protein. *J Phys Chem B.* 2010;114:11909–11919.
25. Aquilina JA, Truscott RJW. Identifying sites of attachment of UV filters to proteins in older human lenses. *Biochim Biophys Acta.* 2002;1596:6–15.
26. Vazquez S, Aquilina JA, Jamie JF, Sheil MM, Truscott RJW. Novel protein modification by kynurenine in human lenses. *J Biol Chem.* 2002;277:4867–4873.
27. Real MD, Ferré J. Biosynthesis of xanthurenic acid 8-O-beta-D-glucoside in Drosophila: characterization of the xanthurenic acid–UDP-glucosyltransferase activity. *J Biol Chem.* 1990;265:7407–7412.
28. Dillon J, Skonieczna M, Mandal K, Paik DC. The photochemical attachment of the O-glucoside of 3-hydroxykynurenine to alpha-crystallin: a model for lenticular aging. *Photochem Photobiol.* 1999;69:248–253.
29. Morandeira A, Engeli L, Vauthey E. Ultrafast charge recombination of photogenerated ion pairs to an electronic excited state. *J Phys Chem A.* 2002;106:4833–4837.
30. Duvanel G, Banerji N, Vauthey E. Excited-state dynamics of donor-acceptor bridged systems containing a boron-dipyrromethene chromophore: interplay between charge separation and reorientational motion. *J Phys Chem A.* 2005;111:5361–5369.
31. Banerji N, Duvanel G, Perez-Velasco A, et al. Excited-state dynamics of hybrid multichromophoric systems: toward an excitation wavelength control of the charge separation pathways. *J Phys Chem A.* 2009;113:8202–8212.

32. Molokov IF, Tsentalovich YP, Yurkovskaya AV, Sagdeev RZ. Investigation of the photo-Fries rearrangement reactions of 1- and 2-naphthyl acetates. *J Photochem Photobiol A Chem.* 1997;110:159–165.
33. Tsentalovich YP, Kulik LV, Gritsan NP, Yurkovskaya AV. Solvent effect on the rate of b-scission of the tert-butoxyl radical. *J Phys Chem A.* 1998;102:7975–7980.
34. Calvert JR, Pitts JN. *Photochemistry*. New-York: John Wiley; 1969.
35. Perdew JP. Density-functional approximation for the correlation-energy of the inhomogeneous electron-gas. *Phys Rev B.* 1986;33:8822–8824.
36. Schäfer A, Horn H, Ahlrichs R. Fully optimized contracted Gaussian-based sets for atoms Li to Kr. *J Chem Phys.* 1992;97:2571–2577.
37. Bauernschmitt R, Ahlrichs R. Treatment of electronic excitations within the adiabatic approximation of time dependent density functional theory. *Chem Phys Lett.* 1996;256:454–464.
38. Ahlrichs R, Bär M, Häser M. Electronic-structure calculations on workstation computers: the program system Turbomole. *Chem Phys Lett.* 1989;162:165–169.
39. Eaton DF. Reference materials for fluorescence measurement. *J Photochem Photobiol B: Biol.* 1988;2:523–531.
40. Benassi E, Sherin PS. Theoretical study of solvent influence on the electronic absorption and emission spectra of kynurenine. *Int J Quant Chem.* 2011;111:3799–3804.
41. Vazquez S, Parker NR, Sheil MM, Truscott RJW. Protein-bound kynurenine decreases with the progression of age-related nuclear cataract. *Invest Ophthalmol Vis Sci.* 2004;45:879–883.
42. Korlimbinis A, Truscott RJW. Identification of 3-hydroxykynurenine bound to protein in the human lens: a possible role in age-related nuclear cataract. *Biochemistry.* 2006;45:1950–1960.
43. Korlimbinis A, Aquilina JA, Truscott RJW. Protein-bound and free UV filters in cataract lenses: the concentration of UV filters is much lower than in normal lenses. *Exp Eye Res.* 2007;85:219–225.
44. Parker NR, Jamie JF, Davies MJ, Truscott RJW. Protein-bound kynurenine is a photosensitizer of oxidative damage. *Free Radical Biol Med.* 2004;37:1479–1489.
45. Mizdrak J, Hains PG, Truscott RJW, Jamie JF, Davies MJ. Tryptophan-derived ultraviolet filter compounds covalently bound to lens proteins are photosensitizers of oxidative damage. *Free Radical Biol Med.* 2008;44:1108–1119.